Contents lists available at ScienceDirect

Applied Catalysis B: Environmental

Enhanced performance for plasma-catalytic oxidation of ethyl acetate over La$_{1-x}$Ce$_x$CoO$_{3+\delta}$ catalysts

Xinbo Zhu [a,b], Shuo Zhang [a], Yang Yang [a], Chenghang Zheng [a], Jinsong Zhou [a], Xiang Gao [a,*], Xin Tu [b,*]

[a] State Key Laboratory of Clean Energy Utilization of Zhejiang University, Hangzhou, 310027, PR China
[b] Department of Electrical Engineering and Electronics, University of Liverpool, Liverpool, L69 3GJ, UK

ARTICLE INFO

ABSTRACT

In this work, plasma-catalytic oxidation of low concentration ethyl acetate (100 ppm) over La$_{1-x}$Ce$_x$CoO$_{3+\delta}$ (x = 0, 0.05, 0.1, 0.3 and 0.5) perovskite catalysts was carried out in a coaxial dielectric barrier discharge (DBD) reactor. The effects of Ce-doping on the removal of ethyl acetate and CO$_x$ (x = 1 and 2) selectivity in the plasma-catalytic oxidation process were investigated as a function of specific energy density (SED). Compared to the plasma reaction without a catalyst, the presence of the LaCoO$_3$ catalyst in the plasma enhanced the removal of ethyl acetate and CO$_x$ selectivity. The use of the Ce-doped catalysts further enhanced the performance of the plasma-catalytic oxidation process. The highest removal efficiency of ethyl acetate (100%) and CO$_x$ selectivity (91.8%) were achieved in the plasma-catalytic oxidation of ethyl acetate over the La$_{0.9}$Ce$_{0.1}$CoO$_{3+\delta}$ catalyst at a SED of 558 J L^{-1}. The interactions between Ce and LaCoO$_3$ resulted in an increased specific surface area (by 17.1%–68.6%) and a reduced crystallite size (by 13.5%–68.2%) of the Ce-doped LaCoO$_3$ catalysts compared to pure LaCoO$_3$, which favours the oxidation of ethyl acetate in the plasma process. Compared to the LaCoO$_3$ catalyst, the Ce-doped perovskite catalysts showed higher content (maximum 54.9%) of surface adsorbed oxygen (O$_{ads}$) and better reducibility, both of which significantly contributed to the enhanced oxidation of ethyl acetate and intermediates in the plasma-assisted surface reactions. The coupling of plasma with the Ce-doped catalysts also reduced the formation of by-products including NO$_2$ and N$_2$O. The possible reaction pathways involved in the plasma oxidation process have been discussed.

© 2017 Elsevier B.V. All rights reserved.

1. Introduction

Ethyl acetate is an organic ester compound, commonly used as a solvent for cleaning electric circuit boards, paint removal and coating. Ethyl acetate easily evaporates, resulting in a large amount being released into the environment, which could cause health problems. Exposure to ethyl acetate even at low concentration may cause nausea, dizziness, irritation and even cancer. Currently, incineration and catalytic oxidation have been the most widely used technologies for the removal of ethyl acetate. However, these technologies are not cost-effective when dealing with the abatement of low concentration ethyl acetate contained in high volume waste gas streams due to the requirement of externally heating large volumes of gas.

Non-thermal plasma (NTP) has been regarded as a promising and attractive alternative to conventional technologies for the removal of a range of low concentration volatile organic compounds (VOCs) in waste gas streams [1,2]. Energetic electrons and highly reactive species including O, O$_3$, N and N$_2$ excited states could be generated in an air NTP even at room temperature, while these energetic species are capable of initiating a variety of chemical reactions, involving direct and indirect destruction of pollutants and intermediates. However, the main challenges in the use of NTP for gas clean-up are the formation of hazardous organic by-products and the relatively low energy efficiency of the plasma process [3,4].

The combination of non-thermal plasma and heterogeneous catalysis has shown great potential to overcome the disadvantages of using NTP alone for gas clean-up and purification. The presence of the catalysts in the plasma could potentially extend the discharge region, offering extra adsorption and active sites for the oxidation of ethyl acetate and driving the reactions with reduced formation of undesirable by-products. This could consequently enhance

the overall performance of the plasma-catalytic oxidation of ethyl acetate in terms of the removal efficiency of ethyl acetate, product selectivity and energy consumption [5,6].

Perovskite-type oxide catalysts have been widely used in thermal catalytic reactions due to their comparative catalytic activity, high thermal stability and low cost. However, very limited perovskite-type catalysts have been explored and investigated in low temperature plasma-catalytic reactions for either gas cleaning or the synthesis of fuels and chemicals. Sun et al. reported that the removal efficiency of toluene was enhanced by ~25% in a $La_{0.8}Sr_{0.2}CoO_3$ catalyst packed dielectric barrier discharge (DBD) reactor at an applied voltage of 21.5 kV compared to that achieved in the reaction using plasma-alone [7]. Dinh et al. also found that the removal of trichloroethylene was increased by over 15% when placing a $LaMnO_3$ catalyst in a plasma reactor at a specific energy density (SED) of 300 J L^{-1}, while the CO_2 selectivity was slightly enhanced [3]. Pahm et al. reported that the reaction selectivity and carbon balance of plasma methane conversion was considerably enhanced when operating in the temperature range from room temperature to 400 °C in the presence of a $LaAlO_3$ catalyst [8].

Recent studies pointed out that partial substitution of A-site of the perovskite catalysts by cations with different oxidation states could result in the formation of structural defects in the catalysts, changing the redox properties of the catalysts and consequently enhancing the catalytic activity. The most popular substitutes for A-site are rare earth, alkali or alkaline earth metals including Sr, Ce, K, Ca and Ba, etc. [9–12]. Among these metals, cerium (Ce) has been widely used as a promoter for catalytic oxidation of VOCs due to its excellent oxygen storage capacity and redox properties between different valences. Previous works have demonstrated that the incorporation of Ce into various perovskite-type catalysts benefits the catalytic oxidation of a variety of pollutants including vinyl chloride [12], benzene [13], methane [14] and even soot [15]. However, the application of Ce-doped perovskite-type catalysts in plasma-induced oxidation of VOCs to enhance the reaction performance of the plasma-catalytic process has not been reported to the best of our knowledge.

In this work, the effect of Ce-doped $LaCoO_3$ catalysts on the plasma-catalytic oxidation of ethyl acetate (100 ppm) was investigated in terms of the removal efficiency of ethyl acetate, CO_x (x = 1 and 2) selectivity and by-product formation in a cylindrical DBD reactor. A range of catalyst characterization, including Brunauer-Emmett-Teller (BET) surface measurement, X-ray diffraction (XRD), X-ray photoelectron spectroscopy (XPS) and temperature programmed reduction of H_2 (H_2-TPR), was performed to get a better understanding of the interactions between Ce-doping and $LaCoO_3$ catalyst and the roles of Ce-doping in the plasma-catalytic oxidation process. The formation of by-products in the plasma-catalytic oxidation process and possible reaction mechanisms behind the plasma oxidation reaction has also been discussed.

2. Experimental

2.1. Catalyst preparation

The $La_{1-x}Ce_xCoO_{3+\delta}$ (x = 0, 0.05, 0.1, 0.3 and 0.5) perovskite type catalysts were prepared by sol-gel method using citric acid as complexing agent and nitrate salts (La, Ce and Co) as precursors. All chemicals were analytic reagent grade (Aladdin Ltd). The desired amount of metal nitrates were firstly dissolved and mixed in deionized water to get 0.1 M solutions. Citric acid with an excess molar ratio of 50% (compared to metal cations) was added to the above solution as a ligand. The solution was vigorously stirred and evaporated in a water bath (80 °C) to get viscous gel. The obtained sample was then dried in an oven at 110 °C overnight followed by calcina-

tion at 700 °C for 5 h. The catalyst samples were pressed and sieved to 35–60 meshes.

2.2. Catalyst characterization

The structural properties of the $La_{1-x}Ce_xCoO_{3+\delta}$ catalysts including specific surface area, average pore size and pore volume were determined via N_2 adsorption-desorption experiments using a Quantachrome Autosorb-1 instrument at −196 °C (77 K). Prior to each measurement, the catalyst samples were degassed at 200 °C for 5 h. The XRD patterns of the catalysts were analyzed by a Rikagu D/max-2000 X-ray diffractometer. The instrument was equipped with a Cu-Kα radiation source, while the scan was conducted in the 2θ range from 10° to 80° with a step size of 0.02°. X-ray photoelectron spectroscopy experiments were performed with a Thermo ESCALAB 250 instrument equipped with an Al Kα X-ray source (hυ = 1486.6 eV) at 150 W. Sample charging effect was calibrated by correcting the obtained spectra with the C1s binding energy (B.E.) value of 284.6 eV. The relative concentrations of cerium ions and oxygen species were calculated based on the areas of the corresponding peaks derived from the XPS spectra of the $La_{1-x}Ce_xCoO_{3+\delta}$ catalysts. The reducibility of the $La_{1-x}Ce_xCoO_{3+\delta}$ catalysts was determined by H_2-TPR using a chemisorption analyzer (Micrometrics, Autochem II 2920). For each test, 50 mg catalyst samples were pre-treated at 250 °C in a N_2 flow for 1 h and cooled down to room temperature. The samples were then heated to 800 °C at a heating rate of 10 °C min^{-1} with a 5 vol.% H_2/Ar flow at a flow rate of 40 mL min^{-1}. The amount of consumed H_2 was calculated by the integration of the peaks in the H_2-TPR profiles.

2.3. Experimental set-up

The experimental set-up consisted of a gas supply system, a DBD reactor, a high voltage power supply, and gas analysis instruments (Fig. 1). Zero grade air (99.999%, Jingong, Hangzhou) was used as a carrier gas in this work. Gaseous ethyl acetate was generated from a gas cylinder (0.5% ethyl acetate, balanced air). All gas streams were regulated by mass flow controllers (Sevenstars D07B, China) and premixed in a mixing chamber before being injected into the DBD reactor. Typically, the experiments were carried out at a total flow rate of 1 L min^{-1}, while the initial concentration of ethyl acetate was 100 ppm. The geometry of the DBD reactor has been described in detail elsewhere [16]; the discharge gap was fixed at 4 mm in this work. 100 mg $La_{1-x}Ce_xCoO_{3+\delta}$ catalyst sample was placed in the plasma region and held in place by quartz wool before each experiment. The length of the catalyst bed was 5 mm. The reactor was connected to an AC high voltage power supply (Suman CTP2000-K, China).

The applied voltage was measured by a high voltage probe (1000:1, Tektronix 6015A), while the voltage across the external capacitor (0.47 μF) was monitored by a voltage probe (Tektronix TPP500). All the electrical signals were sampled by a four-channel digital oscilloscope (Tektronix 3034B). The discharge power was calculated using Q-U Lissajous method. The specific energy density of the plasma process is defined as follows:

$$SED(J \cdot L^{-1}) = \frac{P(W)}{Q(L \cdot min^{-1})} \times 60 \tag{1}$$

where P is the discharge power and Q is the gas flow rate.

Gas analysis was performed by an online multi-component analyzer (Gasmet Dx4000, Finland) with a resolution of 8 cm^{-1}. The analyzer was calibrated with a standard ethyl acetate gas prior to use. The effective path length of the analyzer was 5 m, while the volume of the gas cell was 0.4 L. Measurements were carried out after running the plasma system for about 40 min, when a steady-state had been reached. All the measurements were repeated three
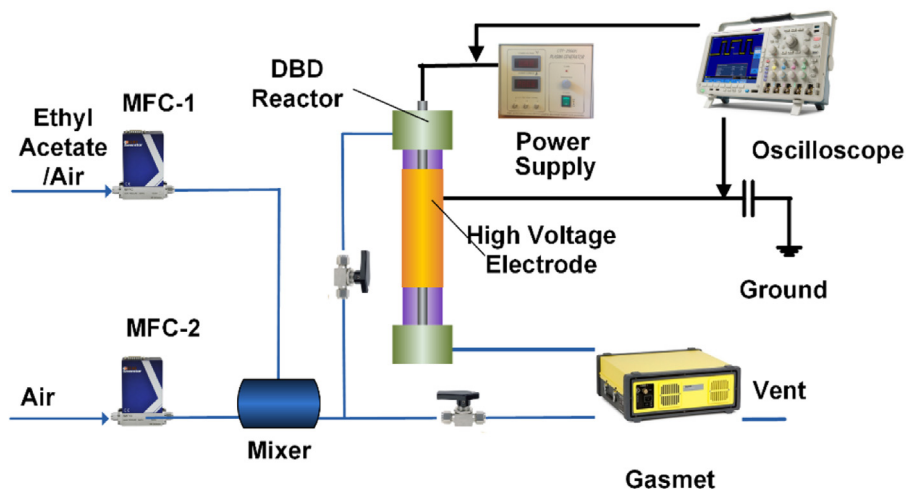
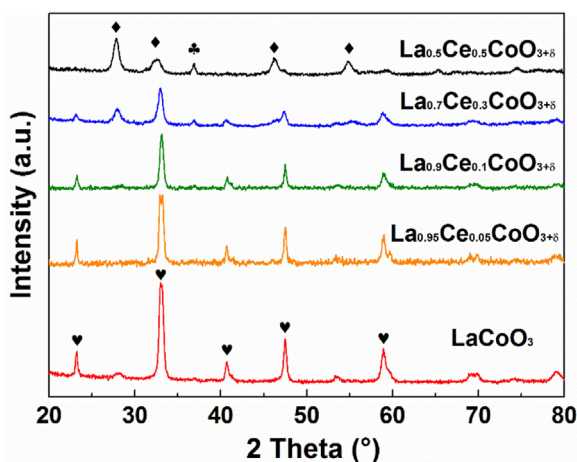**Fig. 1.** Schematic diagram of the experimental set-up.

Fig. 2. XRD patterns of $La_{1-x}Ce_xCoO_{3+\delta}$ catalysts ($\blacklozenge$ CeO_2; $\clubsuit$ Co_3O_4; $\blacktriangledown$ $LaCoO_3$).

times. The removal efficiency of ethyl acetate ($\eta_{\text{ethyl acetate}}$) and CO_x selectivity (S_{CO_x}) of the plasma-catalytic process can be defined as:

$$\eta_{\text{ethylacetate}} = \frac{c_{in} - c_{out}}{c_{in}} \times 100\% \qquad (2)$$

$$S_{CO_x}(\%) = \frac{c_{co} + c_{co_2}}{4 \times (c_{in} - c_{out})} \times 100\% \qquad (3)$$

where c_{in} and c_{out} are the inlet and outlet concentration of ethyl acetate, respectively, while c_{co} and c_{co_2} are the outlet concentration of CO and CO_2.

3. Results and discussions

3.1. Physicochemical properties of the catalysts

Fig. 2 shows the XRD patterns of the $La_{1-x}Ce_xCoO_{3+\delta}$ catalysts. The $LaCoO_3$ catalyst exhibited a typical rhombohedral perovskite structure (JCPDS 25-1060), with the main peak (110) split into two sub-peaks at around $2\theta = 33.0°$. The addition of Ce (x > 0.1) changed the perovskite structure of the $La_{1-x}Ce_xCoO_{3+\delta}$ catalysts as two sub-peaks were merged together, suggesting the formation of a cubic structure of the $LaCoO_3$ catalyst (JCPDS 75-2079). A similar finding was reported in a Sr-doped $LaCoO_3$ catalyst [17]. Phase segregations were expected in the presence of Ce in $LaCoO_3$ catalyst since CeO_2 (JCPDS 34-0394) and Co_3O_4 (JCPDS 42-1467) were observed in the $La_{1-x}Ce_xCoO_{3+\delta}$ samples. Wen et al. also found segregations in Ce-

doped $LaCoO_3$ catalysts when Ce loading was larger than 0.1 [18]. The diffraction peaks of CeO_2 and Co_3O_4 were intensified when increasing Ce content. For the $La_{0.5}Ce_{0.5}CoO_{3+\delta}$ catalyst, no obvious diffraction peaks of perovskite structure were observed; only the characteristic peaks of CeO_2 and Co_3O_4 were present [19].

Table 1 shows the physicochemical properties of the catalysts. Compared to the $LaCoO_3$ catalyst, the introduction of cerium increased the specific surface area (S_{BET}) of the $La_{1-x}Ce_xCoO_{3+\delta}$ catalysts by between 17.1% (x = 0.05) and 68.6% (x = 0.1), suggesting more surface active sites could be formed on the catalyst surface for the oxidation of ethyl acetate. The $La_{0.9}Ce_{0.1}CoO_{3+\delta}$ catalyst showed the largest specific surface area S_{BET} of 11.8 $m^2 g^{-1}$.

3.2. Redox properties of the catalysts

The chemical states of major elements (Ce 3d, Co 2p and O 1s) in the $La_{1-x}Ce_xCoO_{3+\delta}$ catalysts were examined using XPS, as shown in Fig. 3. The binding energy of La $3d_{5/2}$ (837.7 eV) and La $3d_{3/2}$ (834.5 eV) corresponded to pure lanthanum oxides, which indicates that La ions existed in a trivalent form in all the catalysts. No obvious changes were observed with the partial substitution of lanthanum by cerium in the $La_{1-x}Ce_xCoO_{3+\delta}$ catalysts (not shown here).

Fig. 3a shows the Ce 3d spectra of the $La_{1-x}Ce_xCoO_{3+\delta}$ catalysts. The spectra of Ce 3d could be divided into eight peaks corresponding to the spin-orbit splitting. The peaks of Ce $3d_{3/2}$ centred at 900.4 eV, 901.7 eV, 907.2 eV and 916.4 eV were labelled as u, u', u" and u"', respectively, while the peaks of Ce $5d_{3/2}$ located at 882.0 eV, 883.5 eV, 888.4 eV and 897.9 eV were labelled as v, v', v" and v"', respectively. Among the eight peaks, u' and v' peaks corresponded to Ce^{3+} species, while the others belonged to Ce^{4+} [20,21]. The relative concentration of Ce^{3+}, defined as $Ce^{3+}/(Ce^{3+} + Ce^{4+})$, varied from 19.2% to 21.0%, indicating that the majority of surface Ce species formed on the catalyst surface were tetravalent.

The XPS spectra of Co 2p in the $La_{1-x}Ce_xCoO_{3+\delta}$ catalysts (Fig. 3b) showed two main peaks located at around 780.0 eV (Co $2p_{3/2}$) and 795.0 eV (Co $2p_{1/2}$), which is consistent with that reported in previous study [22]. The spectrum of Co 2p can be divided into six peaks. The peaks centred at 780.2 eV and 795.2 eV belonged to Co^{3+}, while the peaks around 781.9 eV and 796.9 eV corresponded to Co^{2+} species [23]. The typical shake-up peaks for Co^{2+} species were found at 790.3 eV and 805.8 eV [24]. The substitution of lanthanum by cerium slightly shifted the binding energies of the $La_{1-x}Ce_xCoO_{3+\delta}$ catalysts towards higher values. The shift of the Co 2p peaks towards higher binding energy could be attributed to the variation of the valences of Co species from trivalent to divalent.

Table 1
Physicochemical properties of $La_xCe_{1-x}CoO_{3+\delta}$ catalysts.

Sample	S_{BET} ($m^2\,g^{-1}$)	La/Co	Ce/Co	Co/(La + Ce + Co)	$Ce^{3+}/(Ce^{3+}+Ce^{4+})$ (%)	$Co^{2+}/(Co^{2+}+Co^{3+})$ (%)	$O_{ads}/(O_{total})$ (%)
$LaCoO_3$	7.0	1.94	–	0.34	–	38.8	49.9
$La_{0.95}Ce_{0.05}CoO_3$	10.6	1.76	0.09	0.35	20.6	40.9	52.1
$La_{0.9}Ce_{0.1}CoO_3$	11.8	1.64	0.29	0.34	21.0	42.3	53.6
$La_{0.7}Ce_{0.3}CoO_3$	9.7	1.52	0.62	0.31	20.3	44.0	51.6
$La_{0.5}Ce_{0.5}CoO_3$	8.2	1.22	0.81	0.33	19.2	46.9	50.2

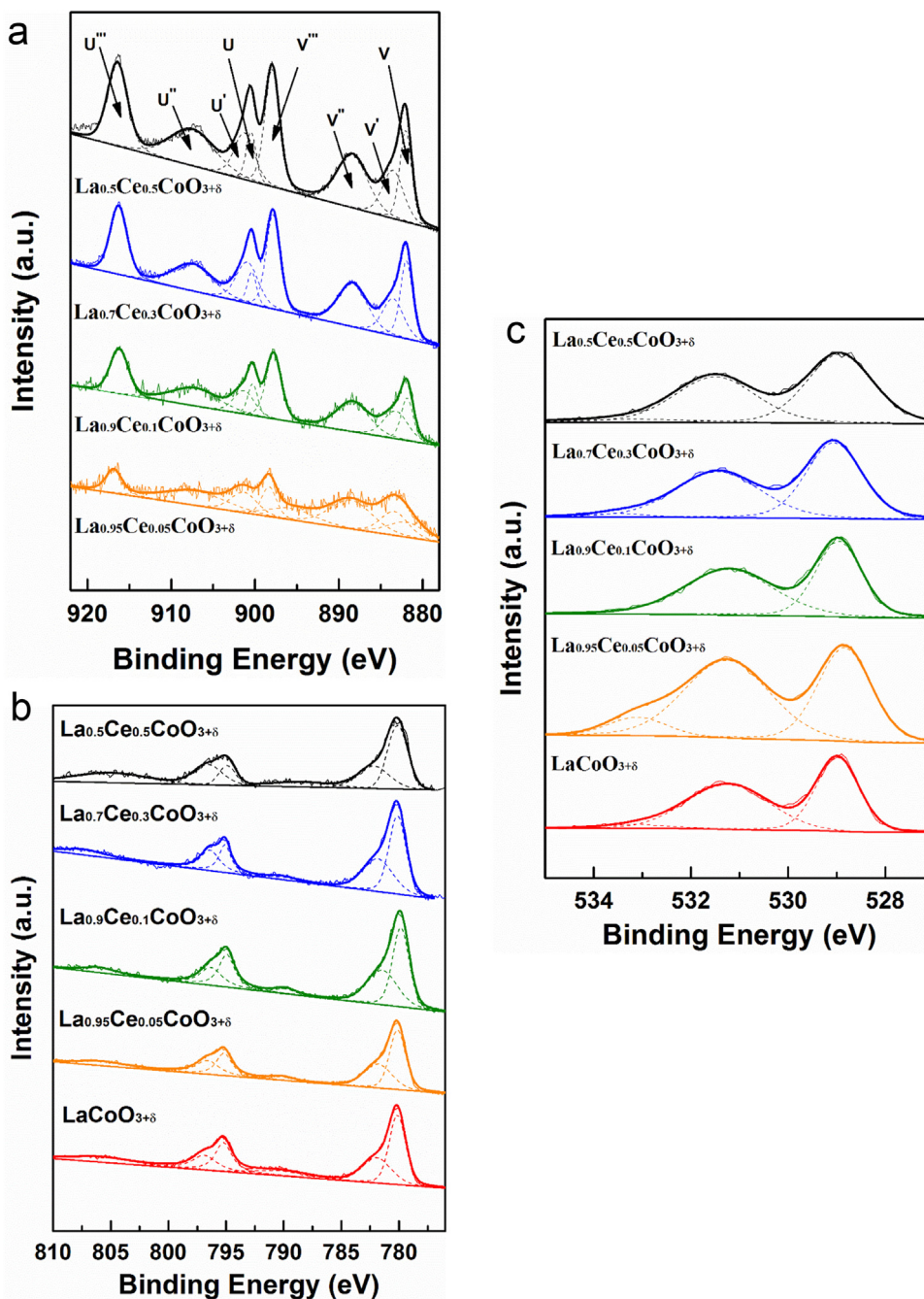**Fig. 3.** XPS spectra of $La_{1-x}Ce_xCoO_{3+\delta}$ catalysts: (a) Ce 3d; (b) Co 2p; (c) O 1s.

With the addition of tetravalent Ce species, a part of Co species become divalent to maintain electronic neutrality in the catalyst structure [18]. This could be confirmed by the increased relative concentration of Co^{2+} species (Table 2).

The O 1s spectra were deconvoluted into three components, as shown in Fig. 3c. The peak at around 531.2 eV was identified as the formation of surface adsorbed oxygen (O_{ads}), while the peak at 528.9 eV was assigned to the generation of lattice oxygen (O_{lat}). In addition, the peak located at around 533.2 eV indicated the
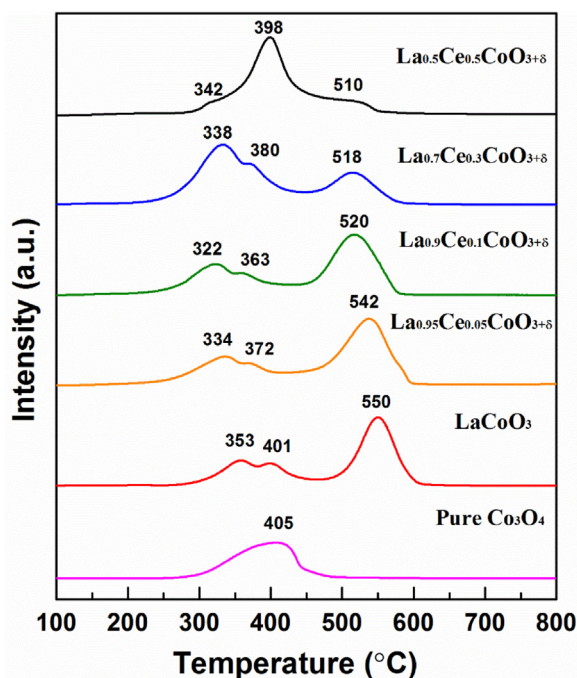
Fig. 4. H_2-TPR profiles of $La_{1-x}Ce_xCoO_{3+\delta}$ catalysts.

Fig. 5. Effect of SED on plasma-catalytic removal of ethyl acetate: (a) removal efficiency of ethyl acetate; (b) CO_x selectivity.

formation of surface adsorbed molecular water [25]. The relative concentration of O_{ads}, defined as O_{ads}/O_{total}, varied from 49.9% to 53.6%. In all the Ce-doped catalysts, the $La_{0.9}Ce_{0.1}CoO_{3+\delta}$ catalyst possessed the highest relative concentration of O_{ads} (53.6%), while further increasing or decreasing Ce doping led to a drop in the relative concentration of O_{ads} formed on the catalyst surface.

The surface atomic ratio of the elements in the $La_{1-x}Ce_xCoO_{3+\delta}$ catalysts was listed in Table 1. The surface enrichment of the A-site element was observed for all samples since the $Co/(La + Ce + Co)$ ratio was between 0.31 and 0.35. This phenomenon could be ascribed to the formation of lanthanum oxides or cerium oxides on the catalyst surface. The missing diffraction peaks of these species could be due to their low quantities [26]. There is no remarkable relationship between the surface enrichment and reaction performance of the plasma process. Wen et al. also reported similar phenomenon in the oxidation of NO over $La_{1-x}Ce_xCoO_3$ catalysts without plasma [18].

The reducibility of the $La_{1-x}Ce_xCoO_{3+\delta}$ catalysts was analyzed using H_2-TPR (Fig. 4). For the $LaCoO_3$ catalyst, three reduction peaks were clearly observed at 353 °C, 401 °C and 550 °C, respectively. The first two peaks can be assigned to the reduction of Co^{3+} to Co^{2+}, while the third peak can be attributed to the reduction of Co^{2+} to elemental Co [27]. The presence of Ce-doping in the $LaCoO_3$ catalyst decreased the reduction temperatures of the $La_{1-x}Ce_xCoO_{3+\delta}$ catalysts as the relevant reduction peaks shifted to lower temperatures. For instance, three reduction peaks of the $La_{0.9}Ce_{0.1}CoO_{3+\delta}$ catalyst were identified at 322 °C, 363 °C, and 520 °C, respectively; lower than those of the $LaCoO_3$ catalyst. Compared to the $La_{0.9}Ce_{0.1}CoO_{3+\delta}$ catalyst, increasing or decreasing Ce-doping affected the reduction of Co^{3+} to Co^{2+} due to the increased relevant reduction temperatures of these catalysts. By contrast, increasing Ce-doping of these catalyst from 0.05 to 0.5 decreased the temperature associated with the reduction of Co^{2+} to Co. Note that the reduction peaks approached the reduction temperature of pure Co_3O_4 (405 °C), which suggests that the segregation of Co species favours the formation of Co_3O_4 as observed in the XRD patterns of the catalysts (Fig. 2) and from the shifting of binding energies of Co 2p in the XPS spectra (Fig. 3).
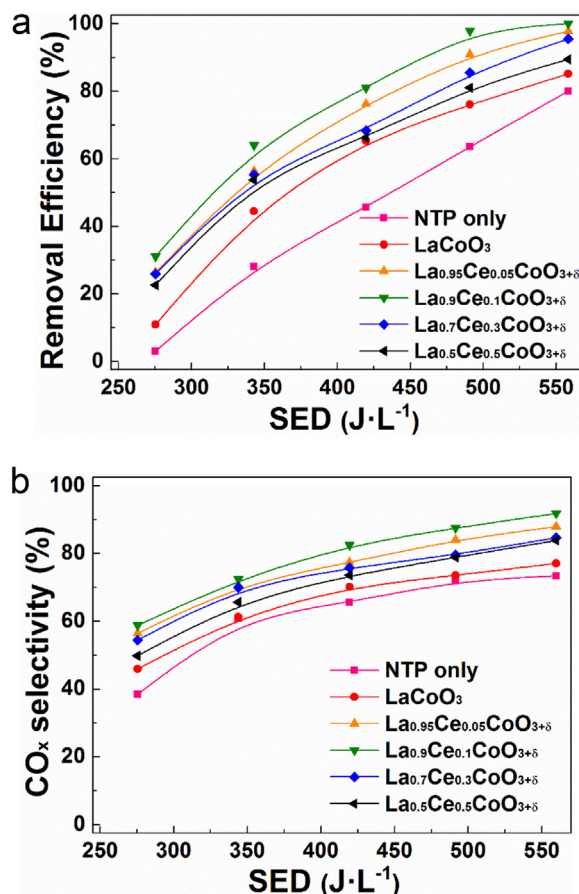
3.3. Plasma-catalytic oxidation of ethyl acetate

Fig. 5 shows the effect of the $La_{1-x}Ce_xCoO_{3+\delta}$ catalysts on the plasma oxidation of ethyl acetate in terms of removal efficiency and CO_x selectivity as a function of SED. The removal of ethyl acetate increased significantly with the increase of SED regardless of the catalysts used. In the plasma oxidation without a catalyst, the removal of ethyl acetate increased from 3.0% to 80.0% when increasing SED from 275 J L^{-1} to 558 J L^{-1}, while the CO_x selectivity increased from 38.4% to 73.4%. It is well known that initially formed energetic electrons generated in non-thermal plasmas interact with the gas molecules present to produce a cascade of processes, leading to the formation of a variety of chemically reactive species including free radicals, excited atoms, molecules and ions. These energetic species are crucial for the initiation and propagation of a variety of chemical reactions for VOC oxidation. Tu et al. reported that the local electric field could be intensified near the contact points of packing materials in a packed bed DBD plasma [28]. The presence of catalyst materials in the DBD plasma could shift the discharge mode to a combination of micro-discharges in the void and surface discharge on the catalyst surface with enlarged discharge area. Increasing SED by changing the applied voltage at a constant gas flow was also reported to increase the number of micro-discharges generated in each discharge cycle, creating more reaction channels, which consequently enhances the generation of the aforementioned reactive species and contributed to the enhanced plasma oxidation of ethyl acetate [25,29]. In typical air plasmas, the major reactive species include O, OH, and metastable N_2 (A). The energetic electrons and highly reactive species have sufficient energy to break the chemical bonds of pollutants (e.g. ethyl

acetate) and convert the pollutants to intermediates. The oxidative radicals (e.g. O) could react with the intermediates, forming final products such as CO, CO_2 and H_2O. The internal energy of the rotational and vibrational excited species could be transferred to the intermediates, accelerating the oxidation of ethyl acetate and intermediates [30].

The integration of the plasma with the $La_{1-x}Ce_xCoO_{3+\delta}$ catalysts significantly enhanced the removal efficiency of ethyl acetate and CO_x selectivity compared to the plasma reaction without a catalyst. The removal of ethyl acetate increased from 10.9% to 85.1% in the tested SED range when placing the pure $LaCoO_3$ catalyst in the DBD, while the CO_x selectivity was enhanced by 35%. Coupling the DBD with Ce-doped catalysts further enhanced the removal of ethyl acetate in the plasma-catalytic reaction. The highest ethyl acetate removal efficiency of 100% and CO_x selectivity of 91.8% were achieved when using the $La_{0.9}Ce_{0.1}CoO_{3+\delta}$ catalyst in the plasma oxidation process at a SED of $558 \, J \, L^{-1}$. The removal efficiency of ethyl acetate and CO_x selectivity followed the order of $La_{0.9}Ce_{0.1}CoO_{3+\delta} > La_{0.95}Ce_{0.05}CoO_{3+\delta} > La_{0.7}Ce_{0.3}CoO_{3+\delta} > La_{0.5}Ce_{0.5}CoO_{3+\delta} > LaCoO_3 >$ plasma-alone over the SED range as shown in Fig. 5.

Catalysts play an important role in determining the performance of plasma-catalytic chemical reactions. The enhanced reaction performance using the Ce-doped catalysts also indicates that there are strong interactions between the dopant Ce and the $LaCoO_3$ catalyst, which in turn affect the plasma oxidation of ethyl acetate. It is well recognized that the specific surface area of a catalyst is closely associated with the density of active sites on the surface of the catalyst for the adsorption of pollutants and intermediates. As shown in Table 1, the specific surface area of the catalysts was improved by between 17.1% and 68.6% by Ce-doping compared to that of the $LaCoO_3$ ($7.0 \, m^2 \, g^{-1}$) catalyst, which should result in more adsorption sites on the surface of the $La_{1-x}Ce_xCoO_{3+\delta}$ catalysts. The residence time of ethyl acetate and intermediates in the plasma reaction region could be prolonged due to the catalyst effect [29]. Thus, the possibilities of effective collisions between ethyl acetate (including intermediates) and chemically reactive species were enhanced over the catalysts with larger specific surface area. Consequently, more efficient utilization of chemically reactive species was expected as these species can be generated both on the catalyst surface and at the interface between gas phase and the catalyst surface [31,32].

The partial substitution of trivalent La^{3+} by tetravalent Ce^{4+} in the A-site of the perovskite structure causes charge imbalance. Electron compensation effect was expected to maintain the electron neutrality and form oxygen vacancies on the catalyst surface [33], which can be evidenced from the presence of Ce^{3+} species on the surface of the $La_{1-x}Ce_xCoO_{3+\delta}$ catalysts. As given in Table 1, the relative content of Ce^{3+} of the $La_{1-x}Ce_xCoO_{3+\delta}$ catalysts decreased from 21.0% to 19.2% when changing the amount of Ce-doping, indicating the decrease of oxygen vacancies on the catalyst surface. Oxygen vacancies are regarded as the adsorption-desorption sites for gas phase oxygen species. Table 1 gives the relative percentage of O_{ads} for all the catalysts. The $La_{0.9}Ce_{0.1}CoO_{3+\delta}$ catalyst showed the highest O_{ads} percentage of 53.6%, whilst the pure $LaCoO_3$ had the lowest (49.9%). The relative concentration of O_{ads} was slightly higher in the catalysts with a low Ce-doping (x = 0.05, 0.1 and 0.3), while further increasing the content of Ce reduced the relative concentration of O_{ads} to 50.2%, This phenomenon could be attributed to the blockage of oxygen vacancies on the surface of $LaCoO_3$ by the segregated CeO_2 and Co_3O_4 phases, considering the lower relative percentage of O_{ads} on pure CeO_2 and Co_3O_4 [16,34]. The presence of oxygen vacancies in the catalysts significantly benefits the generation of surface adsorbed oxygen species (O_{ads}) on the catalyst surface using gas phase oxygen and plasma-generated O species including $O(^3P)$ and $O(^1D)$. The surface adsorbed oxygen (O_{ads})
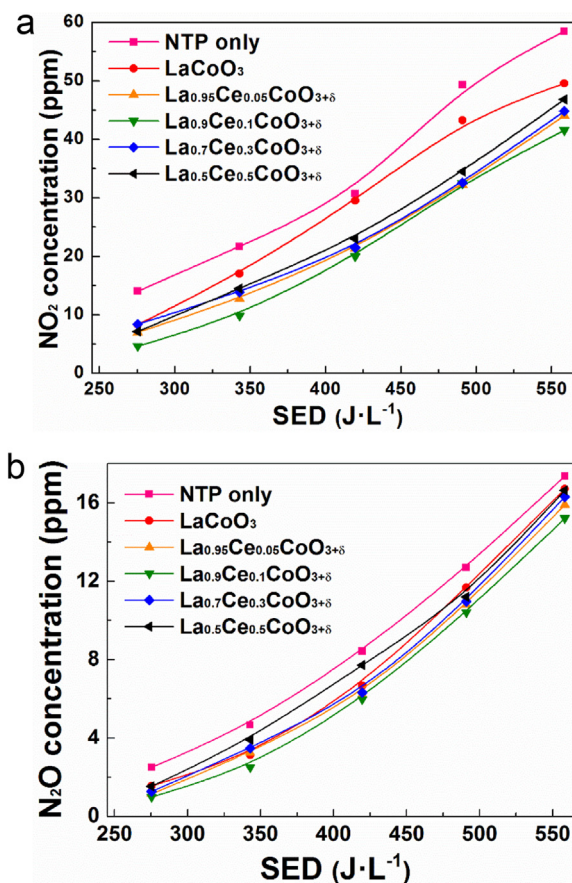
Fig. 6. Effect of SED on the formation of by-products in plasma-catalytic removal of ethyl acetate: (a) NO_2; (b) N_2O.

species play a decisive role in the oxidation of ethyl acetate on the catalyst surface, which could react with the pollutant and intermediates adsorbed on the adjacent sites, forming final products such as CO, CO_2 and H_2O. [35]. At this point, the segregated phases of CeO_2 and Co_3O_4 observed in the $La_{0.7}Ce_{0.3}CoO_{3+\delta}$ and $La_{0.5}Ce_{0.5}CoO_{3+\delta}$ catalysts would have inhibited the formation of oxygen vacancies on the catalyst surfaces (as confirmed by the XPS pattern of O 1s), which in turn inhibited the plasma-catalytic oxidation of ethyl acetate [36]. It should be noted that the reaction performance of the plasma-catalytic process was closely aligned with the relative concentrations of Ce^{3+} and O_{ads} for the $La_{1-x}Ce_xCoO_{3+\delta}$ catalysts in this work.

The redox properties of the catalysts were determined using H_2-TPR. Clearly, Ce-doping significantly affected the redox properties of the $La_{1-x}Ce_xCoO_{3+\delta}$ catalysts. Ce-doped catalysts showed a better reducibility as the reduction temperatures of these catalysts were lower than those of the $LaCoO_3$ catalyst without Ce-doping. This could be attributed to the electron compensation effect caused by the substitution of La^{3+} by Ce^{4+} in the $La_{1-x}Ce_xCoO_{3+\delta}$ catalysts, resulting in the formation of defects and weakened chemical bonds in the perovskite structure of the catalysts. The enhanced oxygen mobility of the $La_{1-x}Ce_xCoO_{3+\delta}$ catalysts contributed to the accelerated surface oxidation of ethyl acetate and intermediates. The sequence of reduction peaks of these catalysts was also consistent with the reaction performances of the plasma-catalytic removal of ethyl acetate.
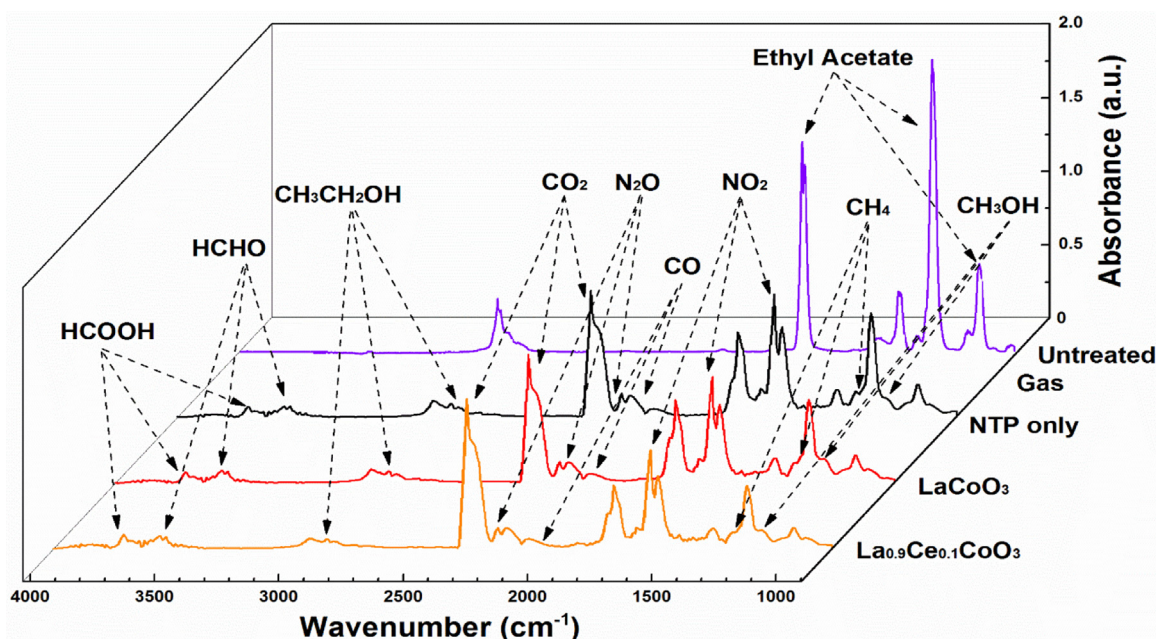
Fig. 7. FTIR spectra of gas phase products in the plasma removal of ethyl acetate at a SED of 491 J L^{-1}.
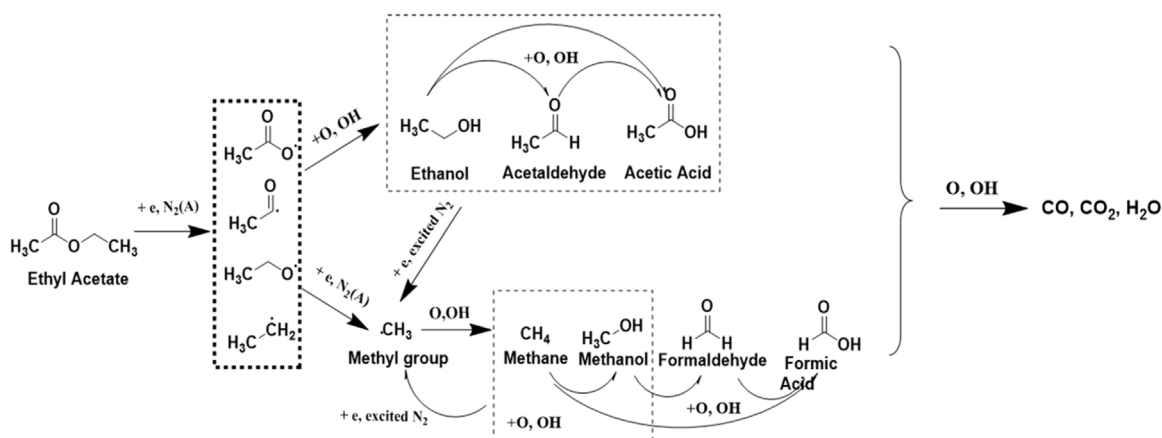

Fig. 8. Possible major reaction pathways in the plasma removal of ethyl acetate.

3.4. Analysis of by-products

In this work, no nitrogen monoxide (NO) was detected under all the experimental conditions. A similar finding was reported by Durme et al. in previous study [37]. Fig. 6 shows the effect of SED on the formation of NO_2 and N_2O in the plasma-catalytic oxidation of ethyl acetate over the $La_{1-x}Ce_xCoO_{3+\delta}$ catalysts. In the plasma oxidation without a catalyst, the concentration of NO_2 increased from 14.0 ppm to 58.5 ppm when increasing the SED from 275 J L^{-1} to 558 J L^{-1}. Clearly, the combination of the plasma with theses catalysts significantly reduced the production of NO_2. For example, the NO_2 concentration varied from 8.3 ppm to 49.6 ppm over the tested SED range when coupling the $LaCoO_3$ catalyst with the DBD; much lower concentrations in comparison to the case in the absence of a catalyst. The presence of the Ce-doped catalysts in the plasma reaction further reduced the formation of NO_2. The lowest NO_2 concentration was achieved when placing the $La_{0.9}Ce_{0.1}CoO_{3+\delta}$ catalyst in the DBD reactor, while the formation of NO_2 was weakly dependent on the amount of Ce present in the catalysts. In addition, the concentration of N_2O produced in the plasma process increased almost monotonically with increasing SED (Fig. 6). N_2O is gener-

ated from the collisions between N and O radicals or the reduction of NO_2. Compared to the plasma reaction without a catalyst, the coupling of plasma with the catalysts reduced the formation of N_2O, while the effect of Ce doping on the formation of N_2O was insignificant in the plasma-catalytic oxidation process.

Fig. 7 shows the Fourier transform infrared (FTIR) spectra of the gas phase products in the plasma processing of ethyl acetate under different conditions (plasma-alone, plasma with $LaCoO_3$ catalyst and plasma with $La_{0.9}Ce_{0.1}CoO_{3+\delta}$ catalyst). CH_3CH_2OH, CH_3OH, CH_4, HCOOH and HCHO were identified as by-products, while CO, CO_2, NO_2 and N_2O were also detected. It is widely recognized that the removal of low concentration pollutants in air plasmas is mainly initiated by direct electron impact reactions and collisions with chemically reactive species including O, N and N_2 excited states. In this study, the energetic electrons could collide with ethyl acetate and carrier gases (N_2 and O_2), forming intermediates and a variety of chemically reactive species. The possible major reaction pathways in the plasma oxidation of ethyl acetate are plotted in Fig. 8. The dissociation energy of C—O bonds in ethyl acetate is 3.38 eV, which is smaller than that of C—C (3.44 eV), C—H (4.29 eV) and C=O (7.55 eV) bonds [38]. Considering the chemical struc-

ture of ethyl acetate, the initial reaction pathways of ethyl acetate decomposition are via breaking of the C—C and C—O bonds, forming ethyl ($CH_3CH_2^\bullet$), acetate ($CH_3COO^\bullet$), acetyl ($CH_3CO^\bullet$), ethoxide ($CH_3CH_2O^\bullet$) and methyl ($CH_3^\bullet$) groups [39]. In a highly chemically reactive plasma environment, most of the C_2 groups would be further decomposed to C_1 species including $CH_3^\bullet$, $CH_2O^\bullet$, CO and CO_2 by electrons or reactive species [40]. Both C_2 and C_1 groups would go through a series of oxidation reactions via collisions with O and OH radicals. As a result, the formation of ethanol, acetic acid and acetaldehyde is possible. Sawyer et al. also reported the formation of ethanol, acetic acid and acetaldehyde as major products in the partial oxidation of ethyl acetate over an alumina catalyst without plasma [41]. However, only ethanol was detected due to the limitation of FTIR in this work. The methyl group ($CH_3^\bullet$) plays a key role in the C_1 chemistry, as it can be oxidized by O and OH to form HCHO or $HCO^\bullet$; these can be further oxidized to generate HCOOH in the presence of O and OH radicals. The formation of CH_4 and CH_3OH could be attributed to the recombination of methyl with H and OH radicals, respectively. A proportion of intermediates and by-products would be oxidized to the final products including CO, CO_2 and H_2O [29]. Both ethyl acetate and the intermediates could be adsorbed onto the surface of the catalysts. In a single-stage plasma-catalytic system, the short-lived reactive species generated near the interface between the $La_{1-x}Ce_xCoO_{3+\delta}$ catalysts and the gas phase could diffuse onto the catalyst surface and participate in the surface reactions. The adsorbed ethyl acetate and intermediates could react with the adjacent oxygen species or hydroxyl groups ($OH^\bullet$) generated from the oxygen vacancies or plasma environment. It is generally recognized that the oxygen species or hydroxyl groups ($OH^\bullet$) driving surface reactions were the major pathways to form the final products of CO, CO_2, H_2O and other organic by-products. The redox cycles between Ce^{4+}/Ce^{3+} and Co^{2+}/Co^{3+} species determine the reducibility of the $La_{1-x}Ce_xCoO_{3+\delta}$ catalysts, which in turn affects the release of surface oxygen species during the surface oxidation of the ethyl acetate and intermediates. As shown in Table 1, the doping of Ce species in the $LaCoO_3$ catalysts increased the relative concentrations of O_{ads} and Ce^{3+}. As a results, the combination of the plasma with the $La_{1-x}Ce_xCoO_{3+\delta}$ catalysts decreased the formation of organic by-products, as evidenced by the enhanced CO_x selectivity (Fig. 5) [42].

4. Conclusions

In this work, the effect of Ce-doped perovskite catalysts on the plasma-catalytic oxidation of low concentration ethyl acetate was investigated in terms of the removal efficiency of ethyl acetate, CO_x selectivity and the formation of by-products. Compared to the plasma reaction in the absence of a catalyst, the integration of the plasma and the $LaCoO_3$ catalyst improved both the removal efficiency of ethyl acetate and CO_x selectivity, while placing the Ce-doped catalysts in the DBD reactor further improved the reaction performance of the plasma-catalytic oxidation process. The highest removal efficiency of ethyl acetate (100%) and CO_x selectivity (91.8%) were obtained when using the $La_{0.9}Ce_{0.1}CoO_3$ catalyst in the plasma at a SED of $558\,J\,L^{-1}$. The doping of Ce on the $LaCoO_3$ catalyst significantly increased the specific surface area of the $La_{1-x}Ce_xCoO_{3+\delta}$ catalysts by 17.1%–68.6% as a result of the interactions between the dopant Ce and $LaCoO_3$. Compared to the properties of pure $LaCoO_3$ catalyst, the Ce-doped catalysts formed more surface adsorbed oxygen (maximum 53.6%) and showed better reducibility with decreased reduction temperatures, as evidenced by the results of XPS and H_2-TPR. All these effects of Ce-doping make a significant contribution to the enhanced removal efficiency of ethyl acetate and CO_x selectivity in the plasma-catalytic oxidation of ethyl acetate. The combination

of DBD with the Ce-doped catalysts also reduced the formation of by-products compared to the plasma process without a catalyst.

References

[1] A.M. Vandenbroucke, R. Morent, N. De Geyter, C. Leys, Non-thermal plasmas for non-catalytic and catalytic VOC abatement, J. Hazard. Mater. 195 (2011) 30–54.

[2] J. Van Durme, J. Dewulf, C. Leys, H. Van Langenhove, Combining non-thermal plasma with heterogeneous catalysis in waste gas treatment: a review, Appl. Catal. B: Environ. 78 (2008) 324–333.

[3] M.T.N. Dinh, J.M. Giraudon, J.F. Lamonier, A. Vandenbroucke, N. De Geyter, C. Leys, R. Morent, Plasma-catalysis of low TCE concentration in air using LaMnO3+δ as catalyst, Appl. Catal. B: Environ. 147 (2014) 904–911.

[4] W. Wang, X. Fan, T. Zhu, H. Wang, D. Ye, X. Hong, Removal of gas phase dimethylamine and N,N-dimethylformamide using non-thermal plasma, Chem. Eng. J. 299 (2016) 184–191.

[5] E.C. Neyts, A. Bogaerts, Understanding plasma catalysis through modelling and simulation—a review, J. Phys. D: Appl. Phys. 47 (2014) 224010.

[6] H.H. Kim, A. Ogata, Nonthermal plasma activates catalyst: from current understanding and future prospects, Eur. Phys. J.-Appl. Phys. 55 (2011) 532–542.

[7] Y.L. Sun, L.B. Zhou, L.H. Zhang, H. Sui, Synergistic effects of non-thermal plasma-assisted catalyst and ultrasound on toluene removal, J. Environ. Sci.-China 24 (2012) 891–896.

[8] M.H. Pham, V. Goujard, J.M. Tatibouet, C. Batiot-Dupeyrat, Activation of methane and carbon dioxide in a dielectric-barrier discharge-plasma reactor to produce hydrocarbons–influence of La(2)O(3)/gamma-Al(2)O(3) catalyst, Catal. Today 171 (2011) 67–71.

[9] A. Mishra, R. Prasad, Preparation and application of perovskite catalysts for diesel soot emissions control: an overview, Catal. Rev. 56 (2014) 57–81.

[10] C. Zhou, Z. Feng, Y. Zhang, L. Hu, R. Chen, B. Shan, H. Yin, W.G. Wang, A. Huang, Enhanced catalytic activity for NO oxidation over Ba doped LaCoO3 catalyst, RSC Adv. 5 (2015) 28054–28059.

[11] Y. Peng, W. Si, J. Li, J. Crittenden, J. Hao, Experimental and DFT studies on Sr-doped LaMnO3 catalysts for NOx storage and reduction, Catal. Sci. Technol. 5 (2015) 2478–2485.

[12] C. Zhang, W. Hua, C. Wang, Y. Guo, Y. Guo, G. Lu, A. Baylet, A. Giroir-Fendler, The effect of A-site substitution by Sr, Mg and Ce on the catalytic performance of LaMnO3 catalysts for the oxidation of vinyl chloride emission, Appl. Catal. B-Environ. 134 (2013) 310–315.

[13] G. Liu, J. Li, K. Yang, W. Tang, H. Liu, J. Yang, R. Yue, Y. Chen, Effects of cerium incorporation on the catalytic oxidation of benzene over flame-made perovskite La1-xCexMnO3 catalysts, Particuology 19 (2015) 60–68.

[14] Y. Shao, X.-F. Wang, M. Ao, C.-R. Gong, G.-L. Fan, H.-F. Chen, Supported La1-xCexMnO3 perovskite catalysts: preparation, characterization and catalytic performance in methane combustion, Front. Mater. Sci. 6 (2012) 304–310.

[15] F. Bin, C. Song, G. Lv, X. Li, X. Cao, J. Song, S. Wu, Characterization of the NO-soot combustion process over La0.8Ce0.2Mn0.7Bi0.3O3 catalyst, Proc. Combust. Inst. 35 (2015) 2241–2248.

[16] X. Zhu, X. Gao, X. Yu, C. Zheng, X. Tu, Catalyst screening for acetone removal in a single-stage plasma-catalysis system, Catal. Today 256 (2015) 108–114.

[17] S.O. Choi, M. Penninger, C.H. Kim, W.F. Schneider, L.T. Thompson, Experimental and computational investigation of effect of Sr on NO oxidation and oxygen exchange for la1-xSrxCoO3 perovskite catalysts, ACS Catal. 3 (2013) 2719–2728.

[18] Y. Wen, C. Zhang, H. He, Y. Yu, Y. Teraoka, Catalytic oxidation of nitrogen monoxide over La1-xCexCoO3 perovskites, Catal. Today 126 (2007) 400–405.

[19] J. Kirchnerova, M. Alifanti, B. Delmon, Evidence of phase cooperation in the LaCoO3–CeO2–Co3O4 catalytic system in relation to activity in methane combustion, Appl. Catal. A: Gen. 231 (2002) 65–80.

[20] Y. Peng, C. Wang, J. Li, Structure–activity relationship of VOx/CeO2 nanorod for NO removal with ammonia, Appl. Catal. B: Environ. 144 (2014) 538–546.

[21] J.Z. Shyu, W.H. Weber, H.S. Gandhi, Surface characterization of alumina-supported ceria, J. Phys. Chem. 92 (1988) 4964–4970.

[22] C. Zhou, Z.J. Feng, Y.X. Zhang, L.J. Hu, R. Chen, B. Shan, H.F. Yin, W.G. Wang, A.S. Huang, Enhanced catalytic activity for NO oxidation over Ba doped LaCoO3 catalyst, RSC Adv. 5 (2015) 28054–28059.

[23] J. Chastain, R.C. King, J. Moulder, Handbook of X-ray Photoelectron Spectroscopy: a Reference Book of Standard Spectra for Identification and Interpretation of XPS Data, Physical Electronics Eden Prairie, MN, 1995.

[24] D. Gu, C.J. Jia, C. Weidenthaler, H.J. Bongard, B. Spliethoff, W. Schmidt, F. Schuth, Highly ordered mesoporous cobalt-containing oxides: structure, catalytic properties, and active sites in oxidation of carbon monoxide, J. Am. Chem. Soc. 137 (2015) 11407–11418.

[25] X. Zhu, X. Gao, R. Qin, Y. Zeng, R. Qu, C. Zheng, X. Tu, Plasma-catalytic removal of formaldehyde over Cu-Ce catalysts in a dielectric barrier discharge reactor, Appl. Catal. B: Environ. 170–171 (2015) 293–300.

[26] C. Zhang, C. Wang, W. Zhan, Y. Guo, Y. Guo, G. Lu, A. Baylet, A. Giroir-Fendler, Catalytic oxidation of vinyl chloride emission over LaMnO3 and LaB0.2Mn0.8O3 (B = Co, Ni Fe) catalysts, Appl. Catal. B-Environ. 129 (2013) 509–516.

[27] P.H.T. Ngamou, N. Kohse-Hoinghaus, N. Bahlawane, CO and ethanol oxidation over LaCoO3 planar model catalysts: effect of the thickness, Catal. Commun. 12 (2011) 1344–1350.

[28] X. Tu, H.J. Gallon, J.C. Whitehead, Transition behavior of packed-Bed dielectric barrier discharge in argon, IEEE Trans. Plasma Sci. 39 (2011) 2172–2173.

[29] E.C. Neyts, Plasma-surface interactions in plasma catalysis, Plasma Chem. Plasma Process. 36 (2015) 185–212.

[30] A.A. Fridman, Plasma Chemistry, Cambridge University Press, 2008.

[31] Y.-R. Zhang, K. Van Laer, E.C. Neyts, A. Bogaerts, Can plasma be formed in catalyst pores? A modeling investigation, Appl. Catal. B: Environ. 185 (2016) 56–67.

[32] F. Holzer, Combination of non-thermal plasma and heterogeneous catalysis for oxidation of volatile organic compounds Part 1. Accessibility of the intra-particle volume, Appl. Catal. B: Environ. 38 (2002) 163–181.

[33] D.Y. Yoon, E. Lim, Y.J. Kim, J.H. Kim, T. Ryu, S. Lee, B.K. Cho, I.S. Nam, J.W. Choung, S. Yoo, NO oxidation activity of Ag-doped perovskite catalysts, J. Catal. 319 (2014) 182–193.

[34] Y. Sun, J. Liu, J. Song, S. Huang, N. Yang, J. Zhang, Y. Sun, Y. Zhu, Exploring the effect of Co3O4 nanocatalysts with different dimensional architectures on methane combustion, ChemCatChem 8 (2016) 540–545.

[35] J.C. Whitehead, Plasma-catalysis: the known knowns, the known unknowns and the unknown unknowns, J. Phys. D: Appl. Phys. 49 (2016) 243001.

[36] N. Nuns, A. Beaurain, M.T.N. Dinh, A. Vandenbroucke, N. De Geyter, R. Morent, C. Leys, J.M. Giraudon, J.F. Lamonier, A combined ToF-SIMS and XPS study for the elucidation of the role of water in the performances of a post-plasma process using LaMnO3 + delta as catalyst in the total oxidation of trichloroethylene, Appl. Surf. Sci. 320 (2014) 154–160.

[37] J. Van Durme, J. Dewulf, W. Sysmans, C. Leys, H. Van Langenhove, Efficient toluene abatement in indoor air by a plasma catalytic hybrid system, Appl. Catal. B-Environ. 74 (2007) 161–169.

[38] C. Zheng, X. Zhu, X. Gao, L. Liu, Q. Chang, Z. Luo, K. Cen, Experimental study of acetone removal by packed-bed dielectric barrier discharge reactor, J. Ind. Eng. Chem. 20 (2014) 2761–2768.

[39] M.R. Nimlos, E.J. Wolfrum, M.L. Brewer, J.A. Fennell, G. Bintner, Gas-phase heterogeneous photocatalytic oxidation of ethanol: pathways and kinetic modeling, Environ. Sci. Technol. 30 (1996) 3102–3110.

[40] W. Sun, M. Uddi, S.H. Won, T. Ombrello, C. Carter, Y. Ju, Kinetic effects of non-equilibrium plasma-assisted methane oxidation on diffusion flame extinction limits, Combust. Flame 159 (2012) 221–229.

[41] J.E. Sawyer, M.A. Abraham, Reaction pathways during the oxidation of ethyl acetate on a platinum/alumina catalyst, Ind. Eng. Chem. Res. 33 (1994) 2084–2089.

[42] E.C. Neyts, K.K. Ostrikov, M.K. Sunkara, A. Bogaerts, Plasma catalysis: synergistic effects at the nanoscale, Chem. Rev. 115 (2015) 13408–13446.